Third International Conference on CFD in the Minerals and Process Industries
CSIRO, Melbourne, Australia
10-12 December 2003

MODELING OF RADIATION INTENSITY IN AN EAF

Diancai GUO and Gordon A. IRONS

Steel Research Centre,
McMaster University
Hamilton, Ontario, Canada L8S 4L7

ABSTRACT

To understand the melting process of steel scrap in an Electric Arc Furnace (EAF), a radiation model has been developed to quantify the radiant energy distribution inside the furnace. Using the operational voltage, current, and power factor, the energy radiated from an arc is determined. Radiation laws are cast into a discretized form to compute the energy intensity inside the furnace. This model enables the separation of the energy received by a surface into the part from each arc and that from the bath surface. The effect of arc length and slag foam height is examined. The energy distributions on sidewall refractory, water-cooled side panels and furnace roof are obtained. Model predictions are in good agreement with industrial observations. The portion of arc energy going into an electrode is examined in detail, and it is found that the value suggested in some publications is too high for modern furnace practice.

NOMENCLATURE

A:	coefficient	nb:	neighbor
a:	area	q:	heat source
Cp:	specific heat	R,r:	resistance / radius
e:	energy	S:	total source term
F:	view factor	T,t:	temperature / time
G:	irradiation	ε:	emissivity
I:	electric current	ρ:	density
J:	radiosity	Γ:	heat conductivity

INTRODUCTION

Electric furnace steelmaking has captured almost half of the world's steel production. Despite its importance, relatively few studies have been carried out to investigate the transport phenomena associated with scrap melting. The present work, on radiation from the arcs, is part of a larger program to investigate the entire process. Other work addresses heating from oxy-fuel burners, scrap movement, melting in the liquid bath and post-combustion.

RADIATION MODEL

Most EAFs operate with 3 graphite electrodes in 3-phase AC at 100 to 400 V and up to 100 MW on the secondary side of a furnace transformer. Measurements are usually made on the primary side of the transformer, including a reactor. The power to the arc is less due to losses in the reactor, in the furnace transformer, and in the bus bar and cables of the secondary circuit. When the electrical resistance and reactance of each of the above-mentioned components are known, the electric resistance of the arc column under a specific operating condition can be obtained.

Once the amount of energy released from an arc is known, the energy radiated from the arc is simply that minus the part directly delivered to the metal bath or scrap in the arc impingement zone, and the part absorbed by the graphite electrode. The estimation of Alexis *et al* (2000) that 18% of the energy release from an arc is directly delivered to the metal bath, has been adopted. It is assumed that 2% of the energy released from an arc absorbed by the electrode. This assumption will be addressed at the end of this paper. From these assumptions, 80% of the energy released from an arc is delivered in the form of radiation; the surrounding slag layer will intercept part of it. The radiation model will determine the distribution of the remainder inside the furnace.

While there are models to compute the temperature of a DC arc (*eg.* Alexis *et al*. (2000)), AC arcs are more complex in that they fluctuate over the cycle, are deflected and precess due to arc interactions and, furthermore, the point of arc attachment moves over the electrode surface. Gu and Irons (1998) employed a channel arc model that showed that the arc could be approximated by a cylinder, or a cone of small conical angle. Therefore, it is assumed that the radiating surface can be well represented by the extended surface of a cylindrical electrode, but deflected outwards from the furnace center. Given the arc length and the amount of radiated energy, the energy flux from this radiating surface is known. This surface is subsequently divided into 72 x 20 (circumference x height) elements, each acts as a black body in radiating, but perfectly transparent in receiving. The movement of the arc is neglected. Furthermore, gas radiation and particle absorption are neglected.

Assuming that the inner surface of the furnace, as well as the top surface of slag or steel, behave as gray body surfaces, for any small area a_i, its radiosity J_i, *i.e.* the energy leaving the area, irradiation G_i, *i.e.* the incident radiant energy, and emissivity ε_i, are related by (Karlekar and Desmond, (1977)):

$$J_i = (1-\varepsilon_i)\cdot G_i + \varepsilon_i e_{bi} \qquad (1)$$

Here the irradiation includes the incident radiation from all radiation sources, such as arcs, bath surface, and walls:

$$G_i = \frac{1}{a_i} \sum_{j=1}^{n-1} a_j F_{j-i} J_j \qquad (2)$$

n is the total number of small areas considered, and F_{j-i} is the view factor between surface a_j and a_i. As the term e_{bi} is related to the temperature of a_i, the net energy gained through radiation can be treated as a source in the energy conservation equation of all control volumes considered. An iterative method is used to find all G_i, and hence J_i, leading to the solution of temperature of the inner surfaces of the panels and roof, the refractory surface, as well as the interior of the refractory wall, based on the SIMPLE scheme (Patankar (1980)),. For these control volumes (CV) the energy, or enthalpy conservation, is given as:

$$\frac{\partial}{\partial t}(\rho C_p T) - \nabla \cdot (\Gamma \cdot \nabla T) = q \qquad (3)$$

in which q is the heat source, including that exchanged by convection and radiation, and the latter is:

$$q_i = G_i - J_i \qquad (4)$$

A code based on previous modeling work on flow and mass transfer (Guo and Irons (2000)), updated with non-orthogonal control volumes, was used to carry out these calculations, and to solve the energy conservation equation.

One feature of the code is that most variables are treated as vectors, such as radiation fluxes, distances, surfaces (with areas projected to the coordinate planes as components). The radiation from one surface to another can be obtained by simple dot multiplication. The calculation of the angles between a surface normal and various connecting lines is thus avoided.

The calculation proceeds as follows. The value of the G function for the furnace internal surface of each related CV is obtained by accumulating the radiation from all other CVs' surface, as shown by Equation (2), and that of J function by Equation (1). These values gives q_i, which is then used in Equation (3) to calculate the temperature of each CV at the next time step. This procedure is repeated to update G_i and J_i, until the total relative error, $\sum \left| (A_{nb} T_{nb} + S_p - A_p T_p) / T_p \right|$, is smaller than 10^{-3} for the whole domain (nb means all neighbor CVs). Then next time step starts.

As a check, the code is used to calculate the radiation from the bath surface of a cylindrical furnace, received by the parallel planes in the freeboard. By setting the bath surface as an ideal emitter, and all the other parts as black bodies at zero temperature, the ratio between the energy received by these planes and the total emitted energy should be equal to the view factor. The calculated results are presented in Figure 1, and compared with analytical solutions published in the literature (Karlekar and Desmond, (1977)). It can be seen that the accuracy of the code is satisfactory.

An industrial furnace is meshed as shown in Figure 2. Electrode 3 is on the left closest to the slag door where slag overflows. The furnace is tapped through a taphole on the other side of the furnace bottom. Basic

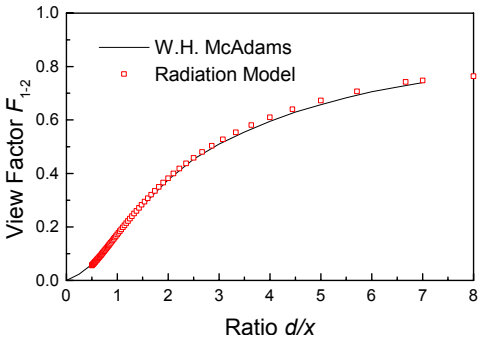

Figure 1: Calculated view factor by the model

assumptions and input values for simulations are summarized in Table 1.

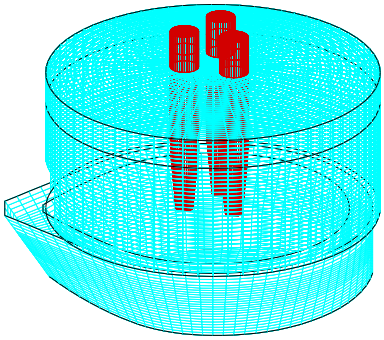

Figure 2 Industrial furnace meshing, tapping side at right.

Modeling Results

Figure 3 gives the radiation intensity from arcs on the sidewalls, including the refractory (immediately above the bath), water-cooled panels (higher in the freeboard) and the vertical part of the roof, "flattened" for presentation. The first contour line from the bottom corresponds to the part of water panels, showing the effect of electrode proximity. Below this line, the part of high intensity corresponds to the refractory wall, as it is closer to the arcs. The contour shape of this zone is due to the irregular shape of the steel bath, and the walls around the slag door (figure centre).

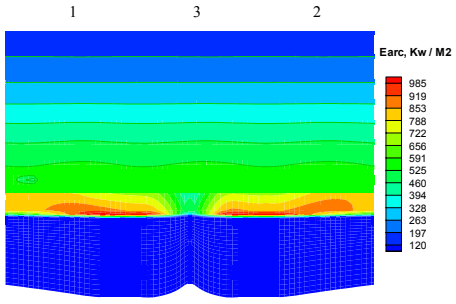

Figure 3: Arc radiation intensity on the sidewalls, H_{slag}=0, L_{arc}=557 mm, $P_{act.}$=94.8 MW.

Table 1: Basic assumptions for numerical simulations

Steel bath depth:	1.26m
Slag layer depth:	0.0 , 0.1, 0.2, 0.3, 0.4 m
Exposed refractory height:	0.4, 0.3, 0.2, 0.1, 0.0 m
Steel bath temperature:	1500, 1550, 1600 °C
Slag top layer temperature:	1600, 1650 °C
Simulated time period:	≥ 2.5 hours to reach the quasi steady state*
Convection coefficient for cooling water	10.0 kW/m^2 K
Convection coefficient for ambient air	2.4, 5, 6 W/m^2 K for bottom, wall and roof
Thickness of panel & roof slag coating	20 mm
Heat conductivity of slag coating	2.2 W/m K
Heat conductivity of refractory	2.4 W/m K
Heat conductivity of insulation layer	0.1 W/m K
Distance from slag top to electrodes	52 to 557 mm
Active power input rate	83.5, 90, 93.6, 94.8 MW

*to be explained in the following

Figure 4 shows the radiation from the steel bath to the sidewalls. The tapping side refractory, being more vertical, receives more radiation than the slag door side (middle of figure). The radiation intensity from the bath is much lower than that from the arcs, about one third in this case.

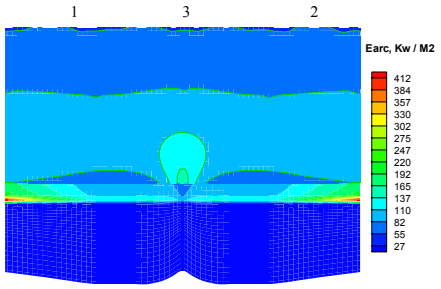

Figure 4 Intensity of radiation from bath surface on the walls, H_{slag}=0, T_{steel}=1500 °C

Figure 5 shows the arc radiation on the steel bath surface. The center region receives the most intense radiation, in the range of about 10 MW/m^2. This intensity means that a 2-mm thick steel sheet, with an emissivity of 0.5, will be melted within 1 second solely by radiation.

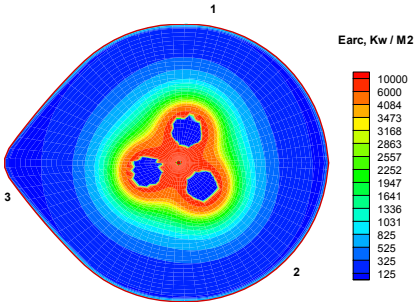

Figure 5 Arc radiation intensity on bath surface, H_{slag}=0, L_{arc}=557 mm, $P_{act.}$=94.8 MW.

The model enables calculation of radiant heat exchange inside an EAF, heat flux calculations, estimations of the hot-face temperature of the slag coating on the water-cooled panels and roof, and so on. Due to the fact that the hot-face temperatures of water-cooled panels and roof, and the temperature distribution in the refractory wall, are not known *a priori*, a transient process was adopted to approach a quasi-steady state for radiation heat exchange. A guessed hot-face temperature distribution for fixed slag and steel temperatures is used to compute the fluxes, and update the temperatures. In this way, the temperatures of refractory, panels and roof gradually approaches a quasi-steady state value. As radiation involves the fourth power of temperature, directly simulating a steady state is not practical, due to poor convergence, and the need of extremely heavy under-relaxation. Figure 6 shows the progress of temperature and irradiation for a monitor CV for one case, indicating that this method indeed leads to a quasi steady state.

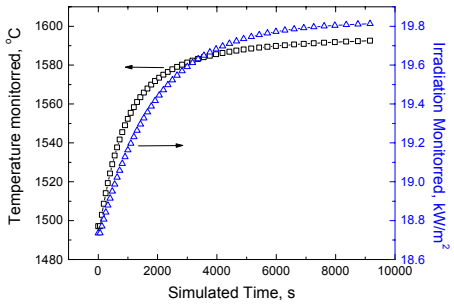

Figure 6 Simulated temperature and irradiation variation of a monitor CV H_{slag} =0.3 m, $P_{act.}$ =93.6 MW, L_{arc}=521 mm.

Figure 7 shows the hot-face temperatures for an exposed arc length of 257 mm. The temperatures are relatively high, refractory hot face above 1700 °C. The protective slag coating on the panels start to melt at temperatures of about 1400 °C.

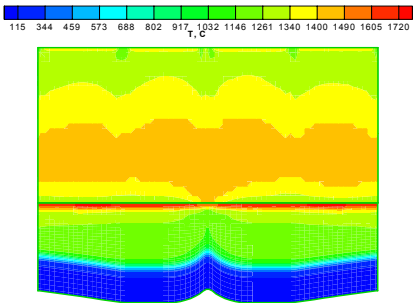

Figure 7 Calculated EAF inner temperature, H_{slag}=0.3 m, T_{slag}=1600 °C $L_{arc\ total}$=557 mm, $P_{act.}$=94.8 MW

All modern EAFs use a foamy slag practice in which carbon monoxide is deliberately evolved to foam up the slag, and bury the arc in the slag. The objectives are to reduce heat losses, refractory erosion and electrical and acoustic noise. Figure 8 shows the effect of varying slag depth on radiative heat exchange for a fixed total arc length of 452 mm. Both the side panels and roof are water cooled, so the heat extracted by cooling water is the sum of those two quantities. The heat absorbed by slag surface and by side panels are most strongly affected by exposed arc length. Under the simulated conditions, the net gain by slag surface becomes negative, as the exposed arc length is less than150 mm, which is the normal operating condition. For the prototype furnace on which these calculations were based, the heat extracted by cooling water varies between 17 and 22 MW in the refining period, while the simulated values are between 12 and 15 MW. Considering that the additional convective heat from the exhaust gas is estimated to be 3 to 6 MW for this period, the agreement is very good.

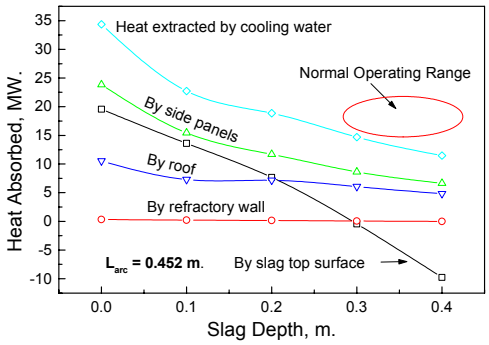

Figure 8 Effect of varying slag depth on radiation heat exchange

ENERGY ABSORBED BY AN ELECTRODE FROM ARC

It has been estimated that about 14% of the total energy released from an arc is dissipated in the electrode (Jordan *et al* (1985), and Ameling *et al* (1986)); however, it is experimentally difficult to verify this figure. The following calculation places an upper bound on this quantity with a simplified steady-state heat transfer calculation.

Assuming that an electrode is working at a steady state, the heat flowing into the electrode from the hot tip, plus the Joule heat generated in the electrode, is balanced by the heat conducted out from the cold end, and that radiated to the surrounding. Therefore, when the temperature distribution of an electrode is known, these heat transfer terms can be easily calculated.

The problem can be conveniently solved as a two-dimensional heat flow problem with non-isotropic, but constant, heat conductivity and electric resistivity. The cylindrical electrode is divided into small control volumes, with finer ones near the hot tip and the outer surface. The heat transfer in an electrode is governed by equation (3), with the additional source term for joule heating:

$$q = I^2 R \tag{5}$$

The electrical current density, due to the "skin effect", is determined by:

$$\frac{I}{I_0} = 0.961 + 0.234\left(\frac{r}{r_0}\right)^4 \tag{6}$$

for an electrode of 610 mm diameter, Orth (1985). The proximity effect of other electrodes is not considered, with I_0 the nominal current density. The physical properties of an electrode and boundary conditions for equation (3) are listed in Table 2. The sublimation temperature of graphite electrode is about 3925 K, and above 3000 K the electrode deteriorates rapidly (Touloukian (1970)). Hot-tip temperatures between 2000 and 3600 K were examined in the calculation. The computation was accomplished with the simple code mentioned earlier (Guo and Irons (2000)).

Table 2 – Physical properties of electrode and Boundary conditions

Electrode Diameter	610 mm
Electrode Length	4 m
Electrical specific resistance, longitudinal	5.2 Ohm.mm^2/m *
Thermal conductivity coefficient, longitudinal	230 W/m K *
Thermal conductivity coefficient, radial	150 W/m K *
AC Current	61500 Amperes
Hot tip temperature	2000-3600 K, 400 K interval
Cold tip temperature	400 K
Emissivity of graphite	0.85
Surrounding temperature	400 K

* (Klein *et al*. (1995))

The calculated temperature distribution for one case is shown in Figure 9. In Figure 10 the surface and centre temperatures of the electrode for the 2 hot-tip temperatures is plotted, showing that most of the temperature variation occurs at the ends, and that beyond 1 meter from the hot tip the temperature stays almost the same for different cases.

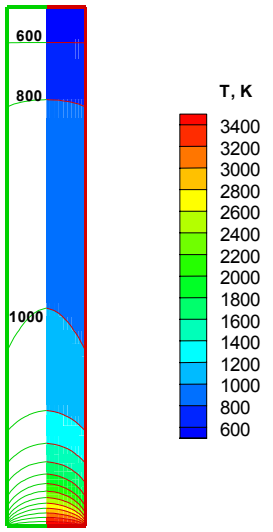

Figure 9 Temperature distribution in an electrode D=610 mm, I=61500 Amp, T_0=3600 °K, $T_{amb.}$=400°K.

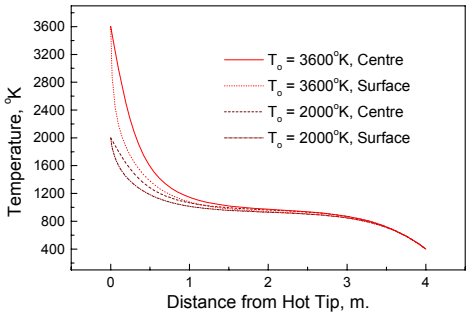

Figure 10: Electrode surface and center temperature D=610 mm, I=61500 Amp, $T_{amb.}$=400 K.

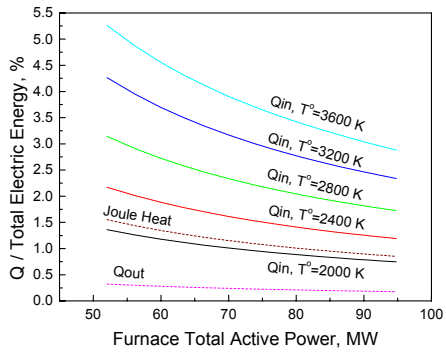

Figure 11: Percentages of exchanged heat over total electric energy D=610mm, I =61500 Amp, $T_{amb.}$=400°K.

The heat transfer terms associated with the electrode are compared with the electric power input in Figure 11. It is clear that the maximum heat flowing into the 3 electrodes from the hot tip, Q_{in}, is less than 5.5% of the total electric energy. Also note that the heat flowing out of the electrode from the cold ends, Q_{out}, is only about 0.2 to 0.3% of the total electric energy under the given conditions, and the Joule heat generated in the electrode is 1 to 1.5%.

To provide a closer estimate of the losses in the electrode there are two quantities in the model to be more precisely defined: the hot-tip temperature and diameter. Examinations of published video recordings of arcs suggest that the hot tip of an electrode (excluding the arcing spot) is usually darker than the steel bath (Jones (1998)). The arcing spot area is small compared to the tip area, which is smaller than the electrode section due to "penciling". Therefore, a hot-tip temperature of 2400 K seems more reasonable, leading to 2% loss, used in the radiation model earlier. Of course, this value needs to be verified experimentally, but it seems much more realistic than 14%.

CONCLUSIONS

A radiation model has been developed to quantify the radiative energy exchange inside an EAF, which enables the separation of radiation from different sources, and the determination of heat extracted by water-cooled panels and roof. It also permits the estimation of the effect of exposed arc length, and hence the slag foaming height, on the refractory walls, and determines the temperature distribution of different parts of the furnace. Calculated energy radiated to water panels and roof is in good agreement with observed values, indicating that the model can be used as a valuable tool in evaluation of EAF furnace design and operational parameter optimization.

Heat transfer analysis of a graphite electrode reveals that with an average hot tip temperature of 3600 K, that no more than 5.5% of the electric energy is absorbed from arc by the electrode at steady state. It is argued that 2400 K is a more reasonable temperature, resulting in a loss of 2%. The heat loss by conduction through an electrode is about 0.3% of the total electric energy for the simulated cases. This value is much less than the Joule heat produced inside the electrode (1 to 1.5%).

REFERENCES

ALEXIS, J., et al, "Modeling of a DC electric arc furnace-Heat transfer from the arc", ISIJ International, Vol. 40, 2000, pp. 1089-1097.

GU, L.P. and IRONS, G.A., 1998, Physical and Mathematical Modeling of Fluid Flow in Electric Arc Furnaces, Electric Furnace Conference Proceedings, vol. 56, Iron and Steel Society of AIME, New Orleans, Nov. 15-18, pp. 411-420.

JONES, R., Private communication, 1998, Mintek, South Africa.

KARLEKAR, B.V. and DESMOND, R.M., "ENGINEERING Heat Transfer", West Publishing Company, New York, 1977, p.240.

PATANKAR, S., "Numerical heat transfer and fluid flow", Hemisphere Publishing Corporation, 1980, New York, p. 126.

GUO, D. and IRONS, G., "Modeling of Gas-Liquid reactions in Ladle Metallurgy: Part II. Numerical Simulation", Metal. & Matls. Transactions, B 31, P.1457, 2000.

JORDAN, G.R., et al, "Basic properties of high intensity electric ARCS used in steel making", British Steel Corporation, ECSC Convention, No. 6210.93/9/801; cited from E. Ploeckinger and O. Etterich, "Electric

Furnace Steel Production", English Translation, John Wiley and Sons, Chichester, 1985, p.131.

AMELING, D., et al, "Untersuchungen zur Schaumschlacken im Electrolichtbogenofen", Stahl und Eisen, 106 (1986), Nr.11, pp.625-630

ORTH, G., "Current displacement in graphite electrodes for arc furnaces" (German), Electrowaerme, B 34, 1976, pp.25-30, cited from E. Ploeckinger and O. Etterich, "Electric Furnace Steel Production", English Translation, John Wiley and Sons, Chichester, 1985, p.130.

TOULOUKIAN, Y.S., et. al, "Thermophysical PROPERTIES of Matter", IFI/Plenum Publication, New York, 1970, Vol. 2, p.23.

KLEIN, R.D., et al, "DC electrodes-a key factor for progress in EAF steel production", Metallurgical Plant and Technology, Vol. 18, 1995, p. 54.